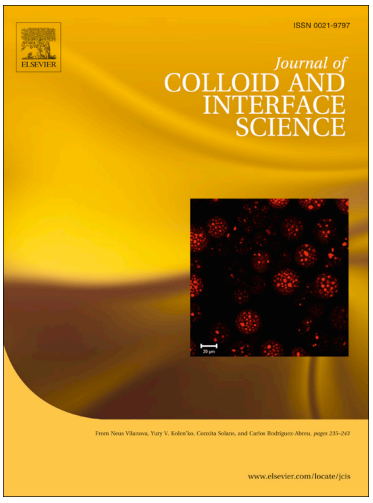

High performance electrochemical glucose sensor based on three-dimensional MoS_2/graphene aerogel

Jae-Min Jeong, MinHo Yang, Dong Seok Kim, Tae Jae Lee, Bong Gill Choi, Do Hyun Kim

PII: S0021-9797(17)30821-4
DOI: http://dx.doi.org/10.1016/j.jcis.2017.07.061
Reference: YJCIS 22590

To appear in: *Journal of Colloid and Interface Science*

Received Date: 22 March 2017
Revised Date: 14 July 2017
Accepted Date: 16 July 2017

Please cite this article as: J-M. Jeong, M. Yang, D. Seok Kim, T. Jae Lee, B. Gill Choi, D. Hyun Kim, High performance electrochemical glucose sensor based on three-dimensional MoS_2/graphene aerogel, *Journal of Colloid and Interface Science* (2017), doi: http://dx.doi.org/10.1016/j.jcis.2017.07.061

High performance electrochemical glucose sensor based on three-dimensional MoS_2/graphene aerogel

Jae-Min Jeong,[a,1] MinHo Yang,[b,1] Dong Seok Kim,[c] Tae Jae Lee,[d] Bong Gill Choi,[b,*] and Do Hyun Kim[a,*]

[a]Department of Chemical & Biomolecular Engineering, KAIST, 291 Daehak-ro, Yuseong-gu, Daejeon 305-701, Republic of Korea

[b]Department of Materials Science and Engineering and Beckman Institute for Advanced Science and Technology, University of Illinois at Urbana-Champaign, Urbana, Illinois 61801, United States

[c]Department of Chemical Engineering, Kangwon National University, Samcheok 25913, Republic of Korea

[d]Nano-Bio Application Team, National Nanofab Center, Daejeon 34141, Republic of Korea

*Corresponding author.

E-mail: bgchoi@kangwon.ac.kr (B.G. Choi), DoHyun.Kim@kaist.ac.kr (D.H. Kim)

Fax: +82-42-350-3910

Tel: +82-42-350-3919

[1]These authors contributed to the paper equally.

Abstract

Two-dimensional (2D) nanosheets have been extensively explored as electrode materials for the development of high-performance electrochemical biosensors due to their unique structural characteristics. Nevertheless, 2D nanosheets suffer from sheet aggregation issues limiting the electrical conductivity of layered metal sulfides or hydroxides. Here, we report high-performance glucose biosensors based on a three–dimensional (3D) aerogel composed of interconnected 2D MoS_2 and graphene sheet. 3D MoS_2/graphene aerogel (MGA) provides a large surface area for the effective immobilization of enzymes, and continuous framework of electrically conductive graphene sheets. Flow-injection amperometric evaluation of the glucose biosensor using a 3D MGA electrode exhibits a rapid response (~4 s), a linear detection range from 2 to 20 mM, a sensitivity of 3.36 μA/mM, and a low limit of detection of 0.29 mM. Moreover, the interference response from oxidizable species, such as, ascorbic acid, uric acid and dopamine is negligible at an operating potential of –0.45 V.

Keywords: Glucose sensor, Graphene, Molybdenum disulphide, 3D gel, hydrothermal, 2D nanosheets, Self–assembly

1. Introduction

Ever-increasing interest in safety, health, and the environment created demand for accurate portable diagnostic devices that can rapidly detect harmful molecules [1]. In this context, electrochemical biosensors are considered to have great potential because they can be incorporated into portable electronic devices, such as, smart phones, and allow users to use them for real time detection [2,3]. To fully satisfy this need, the performances of biosensors must be further improved in terms of selectivity, sensitivity, and response time [4−8]. Electrochemical performance depends greatly on electrode characteristics and can be improved by tailoring effective surface areas, dimensionality, functionality, and ionic and electronic conductivity [9−13]. In this regard, nanostructured materials have been widely used as functional materials for biosensor electrodes because of their large surface areas, short diffusion lengths, enhanced electron transport characteristics, and nanoconfinement effects [14−18].

Two–dimensional (2D) layered nanomaterials, especially monolayer graphene and metal disulfides (MDS), have been utilized as electrode material for electrochemical devices, such as water splitters, lithium ion batteries, supercapacitors, and electrochemical biosensors [19,20]. Among the metal disulfides, 2D molybdenum disulfide (MoS_2) is a promising candidate for the construction of biosensors due to the catalytic activity resulting from many exposed edges similar to functionalized graphene sheets [21,22]. For instance, Wang et al. reported that a MoS_2 nanoparticle-based electrode shows enhanced electrocatalytic activity for the reduction of H_2O_2 [23]. In addition, Huang et al. described that a Cu nanoparticle-functionalized MoS_2 nanosheet exhibits good electrocatalytic behaviour toward glucose detection [24]. However, low electrical conductivity ($< 2.09 \times 10^{-6}$ S/cm) and the stacking

phenomenon limit electron transport and accessible surface area, respectively, and reduce electrochemical performance [24]. To resolve this issue, tremendous efforts have been made to incorporate 2D nanosheets into three−dimensional (3D) porous architectures including, graphene-based aerogels, foams, and sponges. In particular, the graphene framework provides large surface area, improved electrical conductivity, and fast charge transfer, resulting in improved sensing performance [25–27].

Here, we report a one-pot hydrothermal method to prepare 3D MoS_2/graphene aerogels (MGAs) with high electrochemical sensing performance. The various size of porous structure of MoS_2/graphene not only provides large surface areas for enzyme immobilization, but also rapid and efficient transport pathways for ions and electrons. Furthermore, we fabricated a flow-injection biosensor device based on 3D MGA electrodes. The electrochemical biosensors produced in this work showed high sensitivity, low limit of detection, fast response time and high selectivity for the detection of hydrogen peroxide and glucose.

2. Experimental

2.1. Fabrication of 3D MGA

3D MGAs were fabricated using the hydrothermal method. Exfoliated MoS_2 nanosheets were prepared by the lithium intercalation method previously reported [28]. Exfoliated graphene oxide (GO) nanosheets were obtained by oxidation of natural graphite powder according to the modified Hummers method [29]. 8 mL of homogeneous GO aqueous dispersion (3 mg/mL) was mixed with 8 mL of MoS_2 aqueous dispersion (2 mg/mL). After stirring for 1 h, the well dispersed aqueous mixture of GO and MoS_2 was sealed in 18 mL Teflon-lined autoclave and maintained at 180°C for 12 hr for hydrothermal treatment. Finally, the 3D MGA was freeze-dried for one day in order to remove water without destroying its structure.

By contrast, 2D MoS_2/graphene was produced by filtering the mixed solution through anodic membrane filters (25 mm in diameter, 0.2 μm pore size, Whatman) by vacuum suction. And then, 2D MG was ground to powder form at room temperature using a mortar and pestle for 5 min after peeling off from the filter membrane.

2.2. Preparation of glucose oxidase (GOx)/3D MGA electrode

Before modification of GOx/3D MGA electrode, glassy carbon electrode (GCE, dia 1 mm) was polished with 0.05 μm alumina sequentially, and then rinsed with deionized (DI) water. Finally, the electrode was sonicated in ethanol and DI water, dried at room temperature, and ready for modification. Initially, a test tube filled with 3D MGA and 5 ml ethanol ultrasonicated for half an hour to produce a homogeneous solution. Next, a 5 μL of 3D MGA suspension was drop cast on the GCE and left to be dried for almost 15 min. The modified 3D MGA electrode was then immersed in the enzyme solution containing 0.1 M PBS with 2 mg/mL GOx. In order to promote enzyme immobilization, the electrode/enzyme solution was gently agitated for 2 h in a test tube shaker. To prevent enzyme denaturing, the electrode was stored in 0.1 M PBS at 4 ^{o}C prior to electrochemical testing.

2.3. Characterization

We used Rigaku D/max lllC (3 kW) with a θ/θ goniometer equipped with a CuKα radiation generator for X–ray diffraction (XRD) analysis. The diffraction angle of the diffractograms was in the range of 2θ = 5°–80°. The XPS data were collected on a Thermo MultiLab 2000 system with an Al Mgα X–ray source at 200 W. The scanning electron microscopy (SEM) images were obtained using a field emission SEM (Hitachi S–4800 microscope). Transmission electron microscope (TEM) and elemental mapping measurements were carried out using a JEM–2200FS microscope at 200 kV.

2.4. Electrochemical measurements

Cyclic voltammetry (CV) and AC impedance were obtained using VersaSTAT 4 (Princeton Applied Research). For testing purpose, a conventional three-electrode electrochemical cell was used with a glassy carbon working electrode, an Ag/AgCl (3 M KCl) reference electrode, and a platinum wire counter electrode. All potentials were recorded with respect to the reference electrode. AC impedance was measured in the range of 0.01 Hz to 100 kHz at constant amplitude of 10 mV. In order to evaluate the sensing performance, a flow injection system was set up using a syringe pump (KD scientific, KDS 100) and a sample injector (Rhoedyne, model 7725i) with a 20 μL sample loop. The flow electrochemical cell was assembled with working, counter, and reference electrodes in a plastic case. A Teflon gasket with a flow channel was inserted between the working electrode and the plastic case in order to provide sufficient contact between the sample and the GOx (glucose oxidase). The amperometric technique was used in this flow injection system to detect glucose molecules injected at a flow rate of 1 mL/min. All of the electrochemical measurements were performed at room temperature.

3. Results and Discussion

A typical experimental procedure for the preparation of 3D MGAs is described in Fig. 1a. Solution-based exfoliation methods produced stable aqueous colloidal suspension of MoS_2 and GO nanosheets, respectively. After mixing two suspensions, a mixture was highly stable in aqueous solution because both MoS_2 GO nanosheets carry negative charges. A one-step hydrothermal method for 12 hr at 180^{o}C was used to assemble MoS_2 and GO nanosheets into porous structures. After freeze drying, we obtained 3D MGA. Freeze drying process can be formed a lot of macropore from mesopores for hierarchical porous structure with compare supercritical or atmospheric

drying processes [30]. The morphology of 3D MGA was investigated by SEM and TEM (Fig. 1b–d). The 3D MGA was found to have various sizes of pores ranging from the sub–nanometer to several micrometers. High–resolution TEM image (Fig. 1c) confirmed structural stability of composite and coexistence of MoS_2 and graphene. Fig. 1d shows energy–dispersive X–ray spectroscopic (EDS) elemental maps of Mo and S signals for MoS_2 and C signal for graphene, indicating the presence of MoS_2 and graphene throughout the 3D framework. XRD and XPS (Fig. 2a–c) were used to confirm the phases of exfoliated nanosheets. The XRD patterns of bulk MoS_2, as–exfoliated MoS_2 and 3D MGA equally revealed a (002) peak, but a new (001) peak in as–exfoliated MoS_2 and 3D MGA at $2\Theta \approx 7.3°$ indicated an additional separation of 5.5–6 Å between layers during restacking [32]. High resolution XPS revealed two polymorphs (1T and 2H) of MoS_2 from the Mo 3d and S 2p. The binding energy of the 1T phase in 3D MGA was ~0.9 eV lower than the 2H phase of bulk MoS_2 counterpart. This result showed that 3D MGA includes the 1T phase of MoS_2 originated from organolithium exfoliation of MoS_2 [33−35]. In mixture, electrical repulsion between exfoliated MoS_2 and GO nanosheets reduced the restacking rate and led to improvement of ion and electron transfers.

The electrochemical properties of the 3D MGA electrode were evaluated using CV and EIS measurements using a three-electrode system. Analysis of the redox reaction of $Fe(CN)_6^{3-/4-}$ is widely used to investigate the kinetics of redox reactions and the surface features of electrodes [36]. Fig. 3 shows typical CV curves for 3D MGA, GOx/3D MGA, 2D MoS_2/rGO, and GCE electrodes at a scan rate of 50 mV/s. 3D MGA showed a better defined reversible CV curve and higher electrical current with narrower peak–to–peak potential separation (ΔEp, 55 mV) than those of 2D MoS_2/rGO (ΔEp, 113 mV) and bare GC (ΔEp, 92 mV) electrodes, which was

attributed to facilitated ion and electron transport originated from porous and interconnected conductive network. After the immobilization of GOx, peak currents of 3D MGA slightly decreased because the redox reaction was inhibited by the resistance caused by biomolecule adsorption.

Fig. 4a shows the chronoamperograms of the oxidation of $Fe(CN)_6^{4-}$ ions on the RGO/Nafion hybrid and RGO electrodes. The current–time response was governed by the following Cottrell equation [37]:

$$I = FAD^{1/2}C/\pi^{1/2}t^{1/2} \quad (1)$$

where I is the current, F is the Faraday constant, D is the diffusion coefficient, C is the bulk concentration of $Fe(CN)_6^{3-/4-}$, A is the electrode area, and t is the time. The depletion of the electroactive species on the electrode surface leads to an inverse $t^{1/2}$ function. Thus, the diffusion coefficient is the linear relationship of I versus $t^{1/2}$ as shown in Fig. 4b. The diffusion coefficient value of the 3D MGA hybrid was evaluated to be 9.8×10^{-6} cm^2/s from the slopes (Fig. 4b), which is about 3-fold higher than that of the 2D MoS_2/rGO electrode (3.6×10^{-6} cm^2/s). This result elucidates that the GOx/3D MGA electrode promoted the diffusion of ferro/ferricyanide ions into the surface of electrode, compared to the 2D MoS_2/rGO electrode.

Fig. 5 presents CV curves of 3D MGA measured at scan rates of 10 to 400 mV/s. Redox peak currents obviously increased with increasing scan rates. In fact, symmetrical anodic (I_{pa}, R^2 = 0.9964) and cathodic (I_{pc}, R^2 = 0.9975) peak currents were found to be linearly correlated with the square root of the scan rate, indicating a diffusion-confined electrochemical process [39]. In Nernstian or reversible systems, electroactive surface area (A) can be calculated using the Randles-Sevčik equation [37,38]:

$$I_p = (2.69 \times 10^5) n^{3/2} A D_o^{1/2} C_o v^{1/2} \quad (2)$$

where, I_p is the peak current, n is the number of electrons involved in reaction, D_o is the diffusion coefficient, C_o is the concentration, and v is the scan rate. Using this equation, the A value of the 3D MGA electrode was calculated to be 1.36 cm^2, which is higher than that of the 2D MoS_2/rGO electrode (0.98 cm^2) and 3D graphene electrode (Fig. S1, 0.04 cm^2). In addition, the surface coverage (Γ^*) of GOx enzymes on the surface of the 3D MGA electrode was calculated by the following equation [37]:

$$I_p = n^2 F^2 v A \Gamma^* / (4RT)^2 \quad (3)$$

where, n is the number of electrons, R is an ideal gas constant, T is the temperature in Kelvin, F is Faraday's constant and v is the scan rate. Surface coverage of the GOx/3D MGA electrode was 8.32 x 10^{-10} mol/cm^2, indicating an electroactive monolayer of GOx adsorbed on the surface of the 3D MGA (Fig. S2) [39]. As a consequence, the 3D porous and conductive networks provided a large accessible surface area for redox species in the electrolyte and enzyme loadings.

The superior structure of the 3D MGA was further investigated by EIS analysis. Fig. 6 shows typical Nyquist plots for the 3D MGA and 2D MoS_2/rGO electrodes. The charge transfer resistance (R_{CT}) of 3D MGA (75.4 Ω) was much lower than that of 2D MoS_2/rGO (92.35 Ω), suggesting faster electron transfer and indicating that the 3D porous structure accelerated electrochemical kinetics. This enhanced charge transfer is thought to be due to a higher contact area and more efficient electrical connection between the electrolyte and the electrode [40].

The fast ion and electron transfers of the 3D MGA electrode encouraged us to use this structure in an electrochemical biosensor. Another advantage of the 3D MGA electrode is that the integrated MoS_2 acted as an efficient electrochemical catalyst and enhanced the performance of the electrode for glucose detection [11]. Enzyme-based

electrodes for glucose sensors generally detect H_2O_2 molecules generated from the oxidation of glucose by GOx through following reactions [41]:

$$GOx{-}\beta{-}D{-}glucose + O_2 \rightarrow GOx{-}D{-}glucose{-}\delta{-}lactone + H_2O_2 \rightarrow D{-}gluconic\ acid + H_2O$$

$$H_2O_2 \rightarrow O_2 + 2H^+ + 2e^-$$

The electrocatalytic activity of the 3D MGA electrode for the reduction of 0.2 mM H_2O_2 in N_2–saturated PBS solution was also evaluated (Fig. 7). As expected, the 3D MGA electrode had higher catalytic currents for anodic reactions of H_2O_2 (–22 μA) than that of the 2D MoS_2/rGO electrode (–13 μA). We also evaluated the pH-dependent respose of the GOx/3D MGA/GCE. Significantly, elevation of the solution pH led to negative shift of both anodic and cathodic peaks, exhibiting strong pH dependence of the redox reaction of GOx (Fig. S3)

The electrochemical sensing performance of the 3D MGA was evaluated amperometric detection using a flow-injection system. As shown in Fig. 8a, at a polarization potential of –0.45 V, current response increased temporally within 4s and then returned to its original state of the buffer signal level. At all concentrations, the 3D MGA-based biosensor had consistently higher current response than the 2D MoS_2/rGO-based biosensor (Fig. S4). A highly linear current plot was obtained for the 3D MGA-based biosensor at glucose concentrations up to 20 mM (the maximum glucose concentration in real samples) [2]. The limit of detection (LOD) of this biosensor was calculated from signal-to-noise ratio (S/N = 3) as follows [42]:

$$LOD = (k_D S_b)/q_1$$

where, k_D is a factor used for defining the LOD (= 3), S_b is standard deviation of blank signal, and q_1 is the slope of the calibration plot in essential range (2 mM–20 mM). Furthermore, the electrochemical sensing signal of calculated LOD was confirmed in Fig. S4. The response time, defined as the time to reach maximum current, was estimated by averaging response times at different injected glucose concentrations. Background current signal was obtained using PBS solution (Fig. S5). The 3D MGA-based biosensor showed a considerably higher sensitivity (3.36 μA/mM), a lower LOD (0.29 mM), and a faster response time (~ 4 s) than the 2D MoS_2/rGO-based biosensor (Table 1). This sensitivity value of the 3D MGA-based biosensor was higher than those of other biosensors, including layered MoS_2/graphene composite [43], Au modified MoS_2 [44], and MoS_2 nanoparticle [45]. The excellent electrochemical biosensor performance of 3D MGA-based biosensors is attributed to the following characteristics. The interconnected network of MoS_2 exposes large basal planes toward the electrolyte solution at the interface, which enhance H_2O_2 reduction activity of MoS_2 nanosheets via oxygen replacement at exposed Mo edges [46]. The selectivity of a glucose biosensor is one of the most important factors as it avoids interferences common impurities, such as, ascorbic acid (AA), uric acid (UA), and dopamine (DP) (Fig. 8b). The applied potential was optimized at –0.45 V in order to avoid these interferences [46]. A strong current signal for glucose was observed irrespective of the presence of AA, UA, and DP. This indicates that the 3D MGA-based biosensor has excellent glucose selectivity in the presence of the main interfering molecules. In addition, we confirmed the reproducibility of the 3D MGA biosensor by repeating

injection of glucose with same concentration of 4 mM (Fig. S6). The peak currents are almost consistent with an average value of 4.64 μA.

4. Conclusions

We developed a high performance biosensor based on the 3D foam structure of MoS_2 and graphene nanosheets. The 3D MGA electrode was prepared using a simple hydrothermal method. Particularly, the different size of porous structure of the 3D MGA enabled to efficient and rapid pathways for ions and electrons. In order to demonstrate superior features of 3D MGA, two types of electrodes, 3D MGA and 2D MoS_2/rGO, were prepared and their electrochemical performances were intensively characterized. The 3D MGA-based biosensor exhibited better sensing performances than the 2D MoS_2/rGO-based biosensor, in terms of sensitivity, response time, and limit of detection. This result was attributed to large surface area and efficient radial ion diffusion in the 3D MGA structure. The convenient fabrication method used to produce the 3D heterogeneous structure, and the electrochemical performance of the 3D MGC makes these electrodes suitable for producing high sensitivity electrochemical biosensors.

Acknowledgements

This research was supported by Basic Science Research Program through the National Research Foundation of Korea (NRF) funded by the Ministry of Science, ICT & Future Planning (No. 2014R1A5A1009799) and the Ministry of Trade, Industry & Energy (MOTIE), Korea Institute for Advancement of Technology (KIAT) through the Encouragement Program for the Industries of Economic Cooperation Region.

References

[1] L. G. Drummond, M.G. Hill, J.K. Barton, Nat. Biotechnol. 21 (2003) 1192–1199.

[2] J. Wang, Acc. Chem. Res. 35 (2002) 811–825.

[3] X.-Y. Lang, H.-Y. Fu, G.-F. Hou, P. Yang, Y.-B. Liu, Q. Jiang, Nat. Commun. 4 (2013) 1–8.

[4] A. Heller, B. Feldman, Chem. Rev. 108 (2008) 2482–2505.

[5] N. J. Ronkainen, H. B. Halsall, W.R. Heineman, Chem. Soc. Rev. 39 (2010) 1747–1763.

[6] Z. Wang and Z. Dai. Nanoscale 7 (2015) 6420–6431.

[7] R. B. Sadeghian, S. Ostrovidov, J. Han, S. Salehi, B. Bahraminejad, H. Bae, M. Chen, A. Khademhosseini. ACS Sens. 1 (2016) 921–928.

[8] D. G. Rackus, M. H. Shamsi, A. R. Wheeler. Chem. Soc. Rev. 44 (2015) 5320–5340.

[9] Y. Wang, Y. Zhu, J. Chen, Y. Zeng, Nanoscale 4 (2012) 6025–6031.

[10] S. Guo, D. Wen, Y. Zhai, S. Dong, E. Wang, ACS Nano 4 (2010) 3959–3968.

[11] Z. Chen, J. Guo, T. Zhou, Y. Zhang, L. Chen, Electrochim. Acta 109 (2013) 532–535.

[12] P. Si, S. Ding, J. Yuan, X. W. David, D.-H. Kim, ACS Nano 5 (2011) 7617–7626.

[13] C. Xia, W. Ning, Electrochem. Commun. 12 (2010) 1581–1584.

[14] A. Chen and S. Chatterjee, Chem. Soc. Rev. 42 (2013) 5425–5438.

[15] M. B. Wayu, M. A. Schwarzmann, S. D. Gillespie, M. C. Leopold, J. Mater. Sci 52 (2017) 6050–6062.

[16] M. B. Wayu, M. J. Pannell, M. C. Leopold, Chem. Elec. Chem. 3 (2016) 1245–1252.

[17] L. T. DiPasquale, N. G. Poulos, J. R. Hall, A. Minocha, T. A. Bui, M. C. Leopold, J. Colloid Interface Sci., 450 (2015) 202–212.

[18] A. Chen, S. Chatterjee, Chem. Soc. Rev. 42 (2013) 5425–5438.

[19] E. G. S. Firmiano, A. C. Rabelo, C. J. Dalmaschio, A. N. Pinheiro, E. C. Pereira, W. H. Schreiner, E. R. Leite, Adv. Energy Mater., 4 (2014) 1301380–1301388.

[20] G. Zhang, H. Liu, J. Qu, J. Li, Energy Environ. Sci, 9 (2016) 1190–1209.

[21] H. Li, C. Tsai, A. L. Koh, L. Cai, A. W. Contryman, A. H. Fragapane, J. Zhao, H. S. Han, H. C. Mangoharan, F. A.-Pedersen, J. K. Nørskov, X. Zheng, Nature mater. 15 (2016) 48–54.

[22] Q. H. Wang, K. K.-Zadeh, A. Kis, J. N. Coleman, M. S. Strano, Nat. Nanotech. 7 (2012) 699–712.

[23] T. Wang, H. Zhu, H. Zhuo, Z. Zhu, P. Papakonstantinou, G. Lubarsky, J. Lin, M. Li, Anal, Chem. 85 (2013) 10289–10295.

[24] J. Huang, Z. Dong, Y. Li, J. Li, W. Tang, H. Yang, J. Wang, Y. Bao, J. Jin, R. Li. Mater. Res. Bull. 48 (2013) 4544–4547.

[25] H. Hu, Z. Zhao, W. Wan, Y. Gogotsi, J. Qiu, Adv. Mater. 25 (2013) 2219–2223.

[26] Z.-S. Wu, S. Yang, Y. Sun, K. Parvez, X. Feng, K. Müllen, J. Am. Chem. Soc. 134 (2012) 9082–9085.

[27] X. Cao, Z. Yin, H. Zhang, Energy Environ. Sci. 7 (2014) 1850–1865.

[28] J.-M. Jeong, K. G. Lee, S.-J. Chang, J. W. Kim, Y.-K. Han, S. J. Lee, B. G. Choi, Nanoscale 7 (2015) 324–329.

[29] W. S. Hummers, R. E. Offeman, J. Am. Chem. Soc. 80 (1958) 1339.

[30] J. Lu, I. Do, L. T. Drzal, R. M. Worden, I. Lee, ACS Nano 2 (2008) 1825–1832.

[31] A. Ambrosi, Z. Sofer, M. Pumera, Chem. Commun. 51 (2015) 8450–8453.

[32] Z. Sun, Q. Zhao, G. Zhang, Y. Li, G. Zhang, F. Zhang, X. Fan, RSC Adv. 5 (2015) 10352–10357.

[33] M. Acerce, D. Voiry, M. Chhowalla, Nat. Nanotechnol. 10 (2015) 313–318.

[34] R. L. McCreery, Chem. Rev. 108 (2008) 2646–2387.

[35] A. K. Das, C. R. Raj, J. Electroanal. Chem. 140 (2014) 717–718.

[36] A. J. Bard, L. R. Faulkner, Electrochemical Methods: Fundamentals and Applications, Wiley, New York (2001).

[37] E. Laviron, J. Electroanal. Chem. 100 (1979) 263–270.

[38] J. Lu, I. Do, L. T. Drzal, R. M. Worden, I. Lee, ACS Nano 2 (2008) 1825–1832.

[39] B.-Y. Chang, S.-M. Park, Anal. Chem. 78 (2006) 1052–1060.

[40] G. Liu, M. N. Paddon-Row, J. J. Gooding, Electrochem. Commun. 9 (2007) 2218–2223.

[41] J. Mocak, A. M. Bond, S. Mitchell and G. Scollary, Pure Appl. Chem. 69 (1997) 297–328.

[42] K.-J. Huang, L. Wang, J. Li, Y.-M. Liu, Sen. Actuators B 178 (2013) 671–677.

[43] S. Su, H. Sun, F. Xu, L. Yuwen, Microchim. Acta. 181 (2014) 1497–1503.

[44] J. Huang, Y. He, J. Jin, Y. Li, Z. Dong, R. Li. Electrochim. Acta 136 (2014) 41–46.

[45] T. Wang, H. Zhu, J. Zhuo, Z. Zhu, P. Papakonstantinou, G. Lubarsky, J. Lin, M. Li. Anal. Chem. 85 (2013) 10289–10295.

[46] T. F. Jaramillo, K. P. Jørgensen, J. Bonde, J. H. Nielsen, S. Horch, I. Chorkendorff., Science 317 (2007) 100–102.

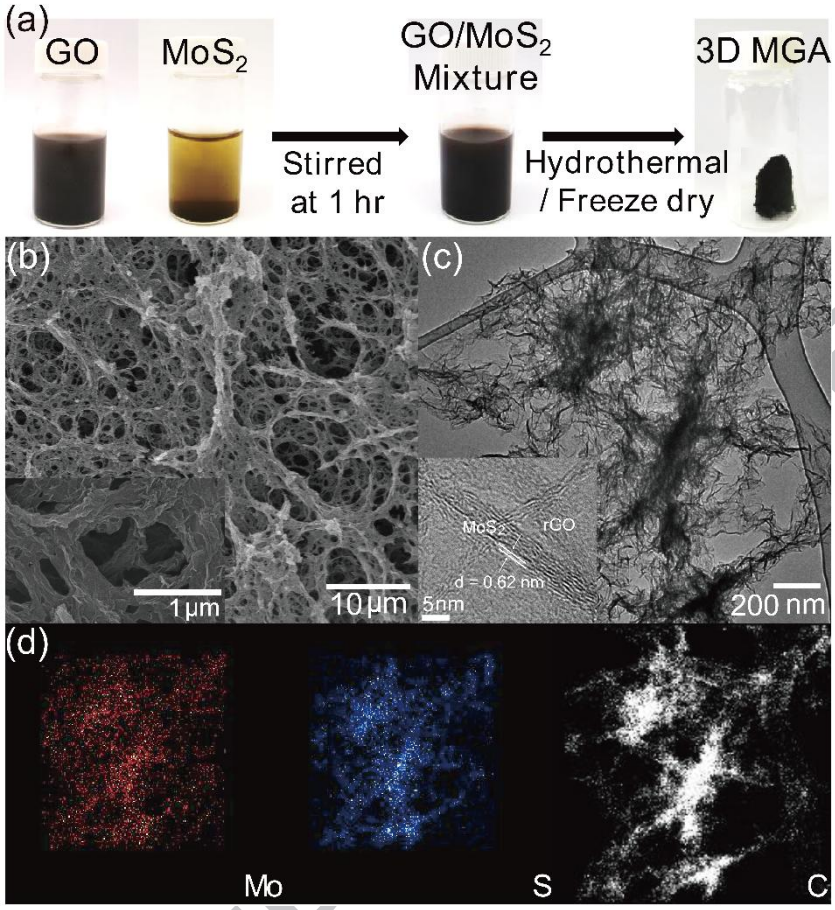

Fig. 1 (a) Typical procedure for the preparation of 3D MGA. (b) SEM and (c) TEM images of interconnected microstructure of 3D MGA. (d) Electron mapping images of Mo, S, and C signals for the 3D MGA.

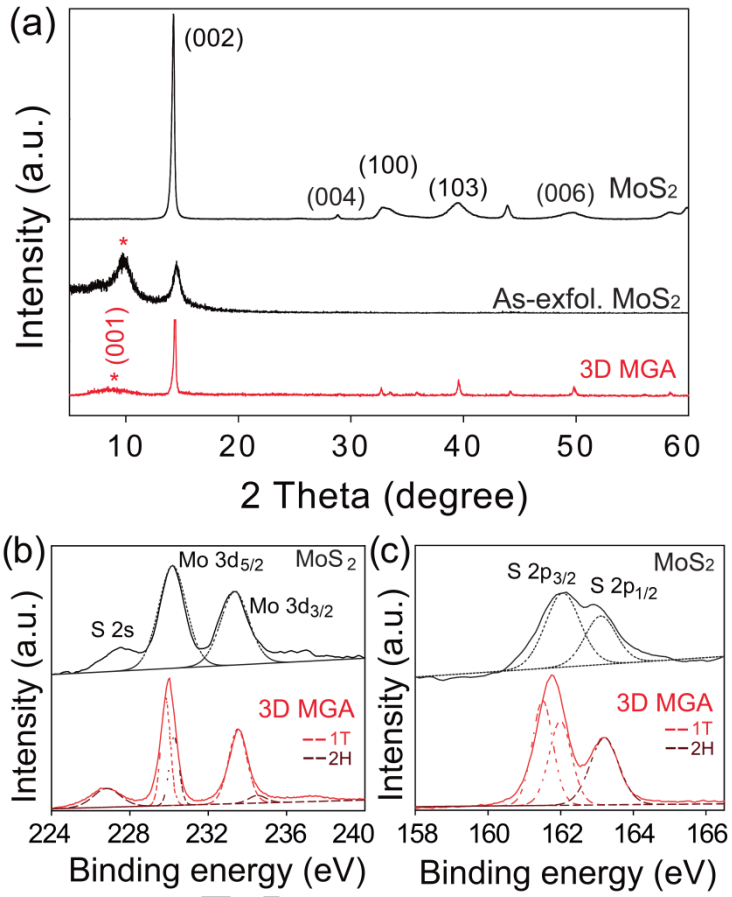

Fig. 2 XRD spectra of MoS_2, as-exfoliated MoS_2, and 3D MGA. (b) and (c) High resolution spectra of Mo 3d and S 2p of 3D MGA compared with bulk MoS_2.

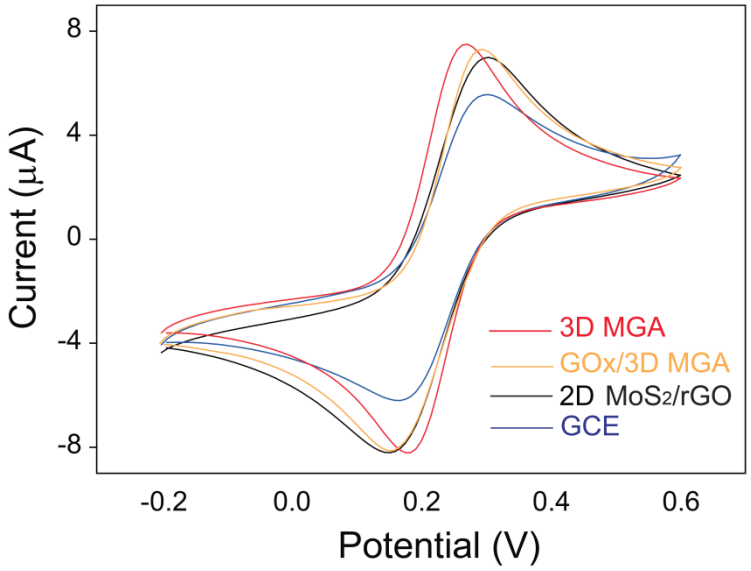

Fig. 3 CV CV curves of the GCE (glassy carbon electrode), 2D MoS_2/rGO, Gox/3D MGA and 3D MGA electrode in a solution of 5 mM $Fe(CN)_6^{3-/4-}$ and 0.1 M KCl..

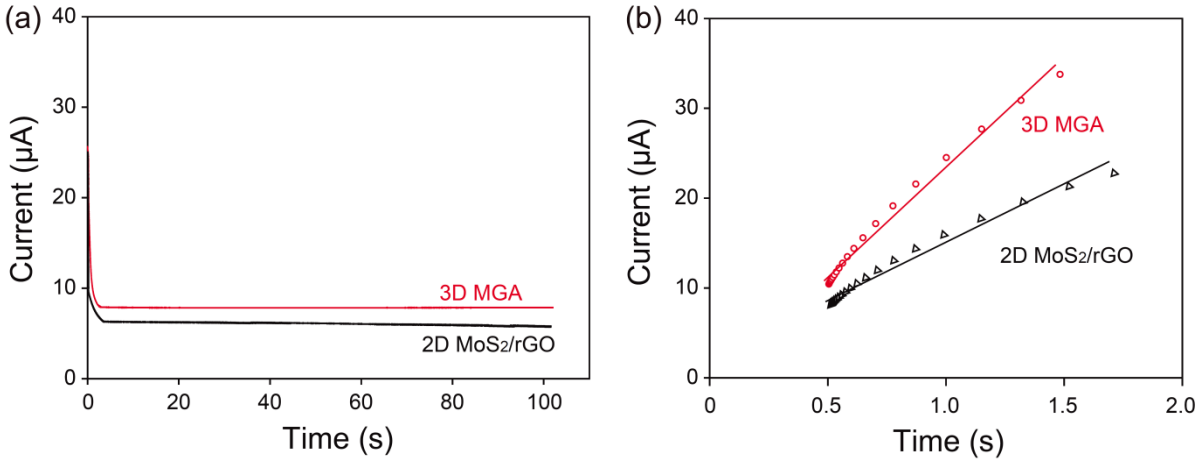

Fig. 4 (a) Chronoamperograms obtained from the oxidation of $Fe(CN)_6^{4-}$ ions with 3D MGA and 2D MoS_2/rGO electrodes and (b) calibration curves of the oxidation current of $Fe(CN)_6^{4-}$ ions vs. $t^{-1/2}$ for 3D MGA and 2D MoS_2/rGO electrodes.

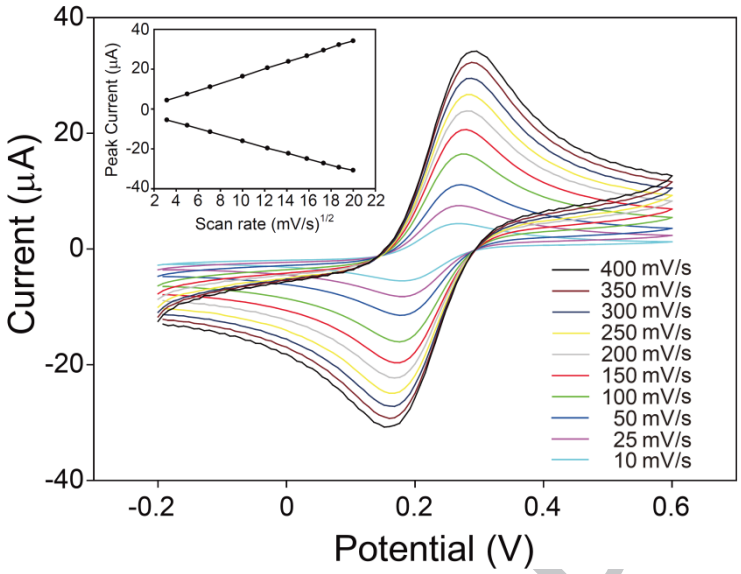

Fig. 5 CV curves of the 3D MGA electrode in sloution containing 5 mM $Fe(CN)_6^{3-/4-}$ and 0.1 M KCl at various scan rates (25, 50, 100, 150, 200, 250, 300, 350, and 400 mV/s).

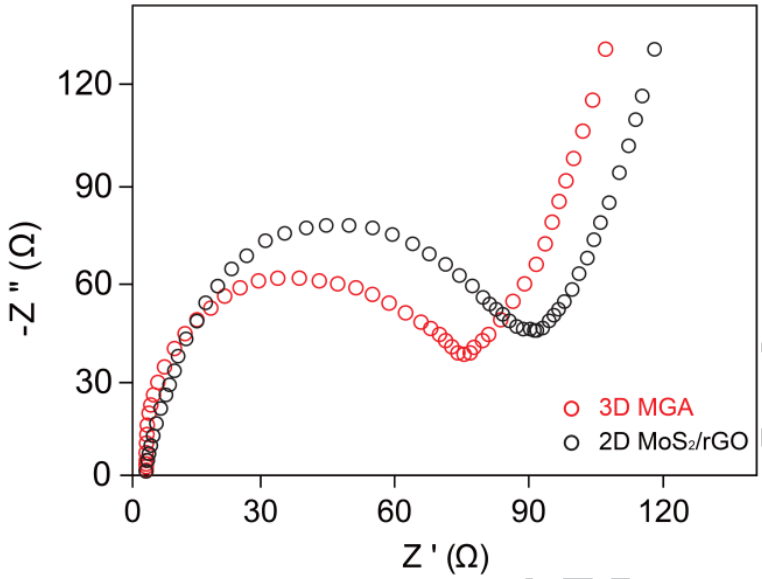

Fig. 6 Nyquist plots of 2D MoS_2/rGO and 3D MGA electrodes with supporting electrolyte solution of 5 mM $Fe(CN)_6^{3-/4-}$ and 0.1 M KCl.

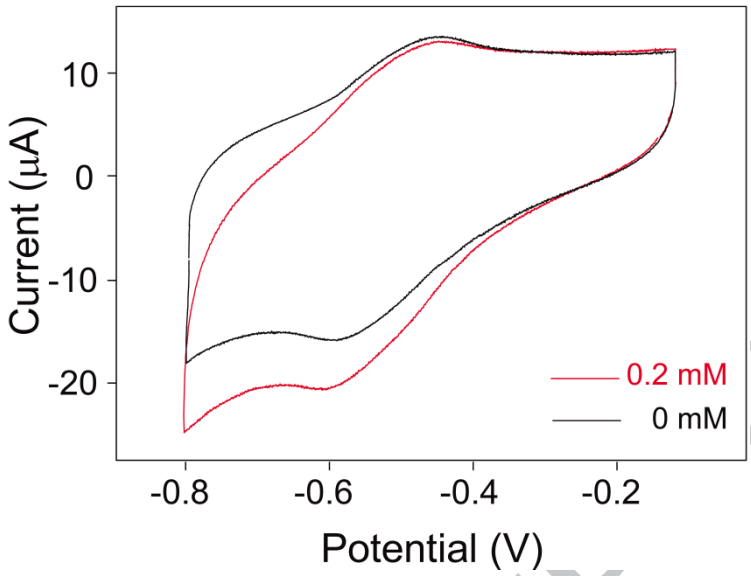

Fig. 7 CVs of 3D MGA electrodes in PBS containing 0.2 mM of H_2O_2 at scan rate of 50 mV/ s.

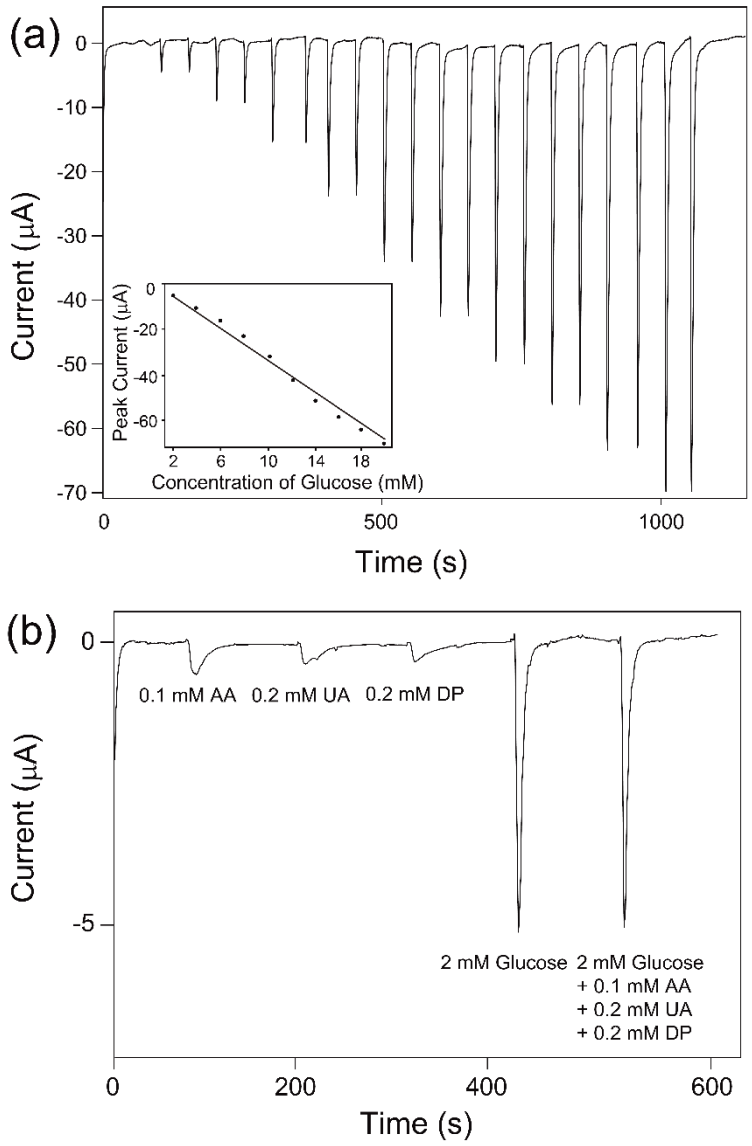

Fig. 8 (a) Amperometric responses of GOx/3D MGA electrode-based fluidic biosensor devices with respect to 2 mM increments of glucose in the flow injection system at –0.45 V. Inset is calibration curve of the electrocatalytic current on the concentration of glucose. (b) Interfering effect of 2 mM glucose, 0.1 mM AA, 0.2 mM UA and 0.2 mM DP on GOx/3D MGA electrode-based fluidic biosensor devices at operating potentials of –0.45 V.

Table 1. Electrochemical performances for GOx/3D MGA and GOx/2D MoS_2/rGO electrode-based biosensors.

Electrode	Sensitivity (μA/mM)	Limit of detection (mM)	Response time (s)	Reference
AuNP@MoS_2/GCE	11.5	2.8	~7	[43]
MoS_2-Gr/GCE	-	0.02	~ 4	[44]
MoS_2 nanoparticle/GCE	2.58	0.0025	~ 5	[45]
3D MGA/GCE	3.36	0.29	~ 4	This work
2D MGA/GCE	0.106	0.92	~7	This work

Supplementary material

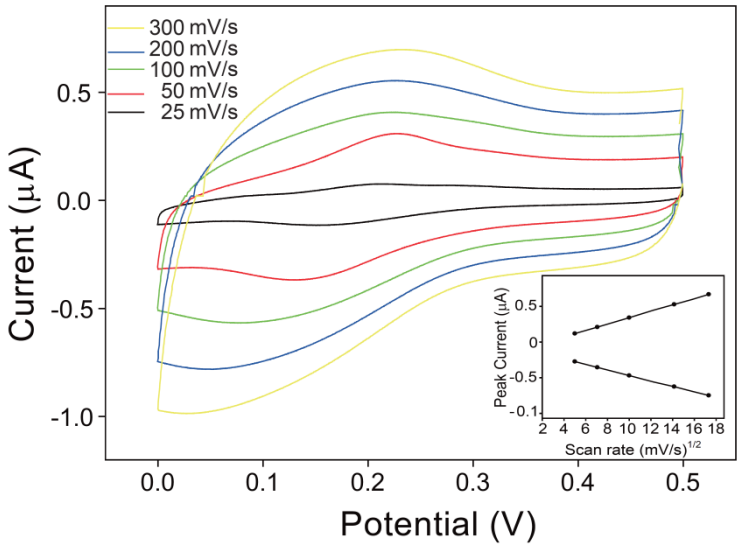

Fig. S1 CV curves of the 3D graphene electrode in sloution containing 5 mM $Fe(CN)_6^{3-/4-}$ and 0.1 M KCl at various scan rates (25, 50, 100, 200, and 300 mV/s).

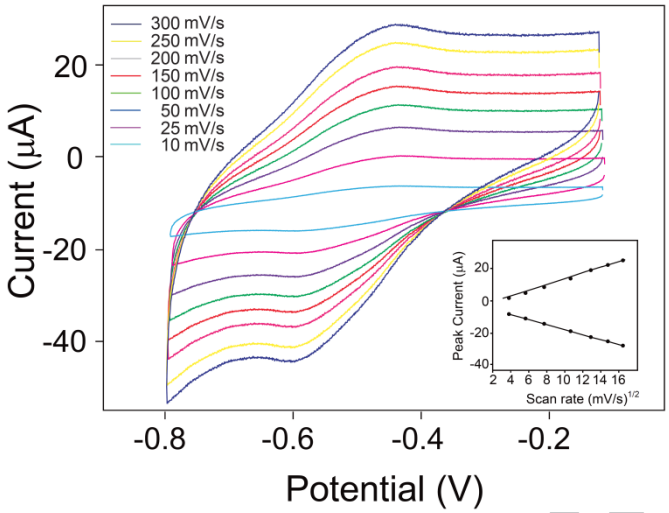

Fig. S2 CV curves of the GOx/3D MGA electrode in sloution containing glucose and PBS buffer solution at various scan rates (25, 50, 100, 150, 200, 250 and 300 mV/s).

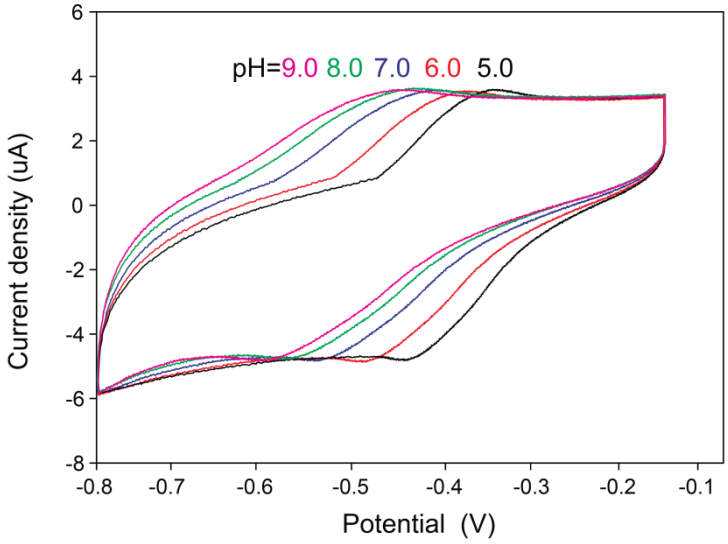

Fig. S3 CV curves of the GOx/3D MGA electrode in PBS buffer with different pH values (9.0, 8.0, 7.0, 6.0 and 5.0),

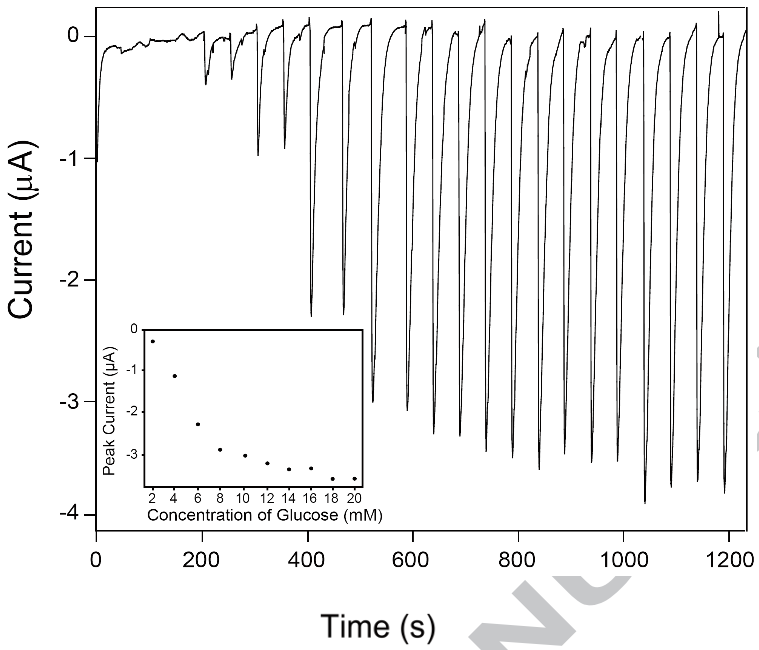

Fig. S4 Amperometric responses of GOx/2D MoS_2/rGO electrode-based fluidic biosensor devices with respect to 2 mM increments of glucose in the flow injection system at –0.45 V. Inset is calibration curve of the electrocatalytic current on the concentration of glucose.

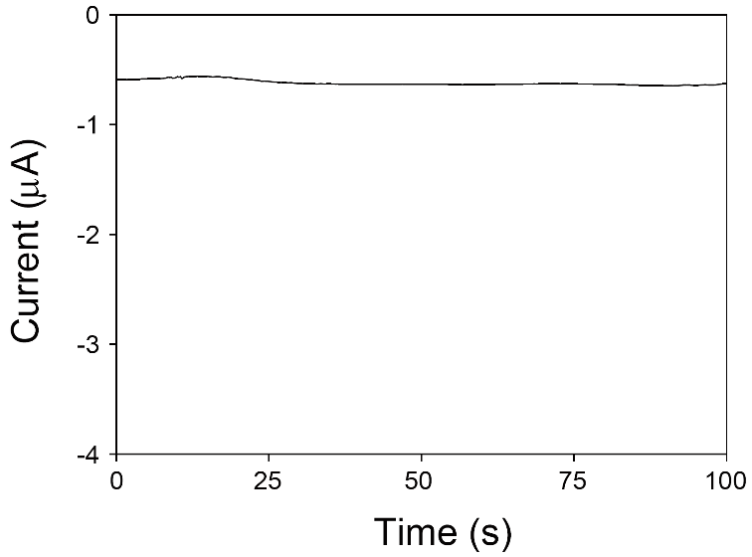

Fig. S5 Background current of GOx/3D MGA biosensor using PBS solution in the flow injection system at –0.45 V.

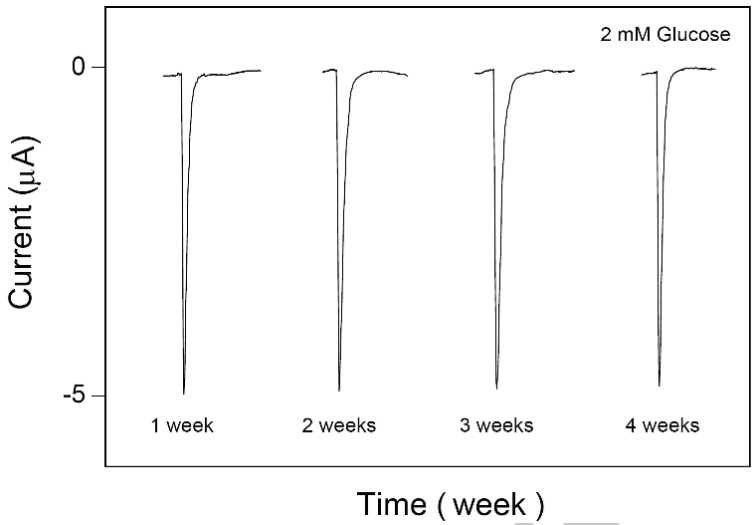

Fig. S6 Amperometric responses of GOx/3D MGA electrode-based fluidic biosensor by repeating 4 weeks injection of glucose with concentration of 2 mM at –0.45 V.

Graphical abstract

Three–dimensional MoS_2/graphene aerogel was prepared by a hydrothermal and freeze drying method, demonstrating great potential as a sensing electrode for detecting glucose with high sensitivity, low detection limit, and high selectivity.